Spontaneous generation of spiral waves by a hydrodynamic instability

Habibi, M.; Møller, P.C.F.; Ribe, N.M.; Bonn, D.

Published in:
Europhysics Letters

DOI:
10.1209/0295-5075/81/38004

A Letters Journal Exploring the Frontiers of Physics

February 2008

EPL, **81** (2008) 38004
doi: 10.1209/0295-5075/81/38004

www.epljournal.org

Spontaneous generation of spiral waves by a hydrodynamic instability

M. Habibi[1,2], P. C. F. Møller[1], N. M. Ribe[3] and D. Bonn[1,4]

[1] *Laboratoire de Physique Statistique, UMR 8550 CNRS, École Normale Supérieure - 24, rue Lhomond, 75231 Paris Cedex 05, France*
[2] *Institute for Advanced Studies in Basic Sciences (IASBS) - Zanjan 45195-1159, Iran*
[3] *Institut de Physique du Globe de Paris and Université de Paris-7, CNRS, Tour 14 - 2, place Jussieu, 75005 Paris, France*
[4] *Van der Waals-Zeeman Institute, University of Amsterdam - Valckenierstraat 65, 1018 XE Amsterdam, The Netherlands*

received 25 April 2007; accepted in final form 4 December 2007
published online 3 January 2008

PACS 83.60.Wc – Flow instabilities
PACS 47.54.-r – Pattern selection; pattern formation
PACS 47.35.-i – Hydrodynamic waves

Abstract – The coiling of a thin filament of viscous fluid falling onto a surface is a common and easily reproducible hydrodynamic instability. Here we report for the first time that this instability can generate regular spiral patterns, in which air bubbles are trapped in the coil and then advected horizontally by the fluid spreading on the surface. We present a simple model that explains how these beautiful patterns are formed, and how the number of spiral branches and their curvature depends on the coiling frequency, the frequency of rotation of the coiling center, the total flow rate, and the thickness of the spreading fluid film.

The study of spirals in Nature goes back at least to the seventeenth century, when Swammerdam was among the first to describe the beautiful forms of certain seashells [1]. The standard work on spontaneous pattern formation in Nature, D'Arcy Thompson's *On Growth and Form* [1] describes a multitude of spiral patterns, including those of shells, sunflower seeds, and the helical structure of branches or leaves on growing plant stems. All these spirals are self-organized and obey rather strict mathematical rules. Shells, for example, are generally logarithmic spirals in which the distance between successive loops grows in a precisely determined way with increasing distance from the center [2]. In the case of sunflower seed spirals (phyllotaxis), Douady and Couder [3] used a clever laboratory experiment to show that the spirals form due to a self-organized growth process whereby new seeds are generated in the center at a fixed frequency and then repel each other by steric repulsion. The maximization of the distance between the seeds then leads to a special subtype of the logarithmic spiral pattern: the golden or Fibonacci spiral. The same authors showed how these ideas can be applied to plants, accounting for instance for the sunflower spirals [4].

Not all natural spirals are due to a steric repulsion between constitutive elements, however. Over the past few years, self-organized spiral waves have been studied extensively [5]. These dynamic spirals form spontaneously in excitable media [6,7] and have been observed in contexts as different as catalytic surface oxidation [8], the Belousov-Zhabotinsky chemical reaction [9–13], aggregating colonies of slime mold [14,15] and contracting heart tissue, where such waves are believed to be related to cardiac arrhythmia and fibrillation [16].

Here we demonstrate that spirals can also arise during the coiling of a thin "rope" of viscous fluid falling onto a solid surface (fig. 1) [17–19]. In previous papers we investigated how the frequency and radius of the coiling depends on the orifice diameter, the height of fall, the flow rate, and the fluid viscosity, and we showed that coiling traverses four different dynamical regimes as the fall height increases [20–24]. Here we report that in a limited portion of the parameter space, air bubbles become trapped between successive coils and are then advected radially away to form surprising and very regular spiral patterns. We also present a simple model that explains how these beautiful patterns are formed, and

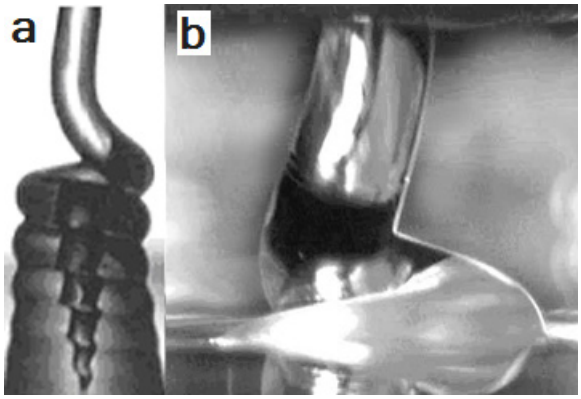

Fig. 1: Liquid rope coiling. Depending on the fluid viscosity, the coils can either build up a tall pile like a corkscrew (a), or vanish into the bulk of the fluid within one coiling period (b). a) silicone oil with $\nu = 1000\,\mathrm{cm}^2/\mathrm{s}$, injected from an orifice of radius $a_0 = 0.034\,\mathrm{cm}$ at a volumetric rate $Q = 0.0044\,\mathrm{cm}^3/\mathrm{s}$. Effective fall height $H = 0.5\,\mathrm{cm}$. The diameter of the portion of the rope shown is 0.06 cm. b) Silicone oil with $\nu = 125\,\mathrm{cm}^2/\mathrm{s}$, falling from an orifice of radius $a_0 = 0.2\,\mathrm{cm}$ at a flow rate $Q = 0.1\,\mathrm{cm}^3/\mathrm{s}$. The fall height is 1.5 cm. The diameter of the portion of the rope shown is 0.4 cm.

how the number of spiral branches and their curvature depends on the total flow rate, the fluid film thickness, and ratio of the coiling frequency to the frequency of precession of the coiling center. We find that the spiral waves occur only when the center of the coil precesses with a frequency that is distinct from that of the coiling itself, and we show that this condition is both necessary and sufficient for the appearance of Fermat spirals in this particular case. This is in contrast to the general case where for instance the standard type ($n = 1$) of Archimedean spiral wave patterns forming in excitable media can exist with a single frequency, which is the primary rotation frequency of the spiral, or alternatively form non-static spirals with two frequencies resulting in a well-studied meandering instability that causes the spiral wave tip to trace out epicycloid trajectories (see for example [5]). The second frequency associated with the meandering instability is generally incommensurate with the primary rotation frequency, which can be formally eliminated by transformation to a co-rotating frame in which the stable rigidly rotating spirals appears stationary. In our experiments the two frequencies are also generally incommensurate, but the second frequency plays a quite different role than in the meandering spirals.

We performed our experiments by ejecting a thin jet of silicone oil from a syringe, driven by a syringe pump with a computer-controlled stepper motor. In a typical experiment, the fluid was ejected continuously at a constant rate Q while the fall height H was varied over a range of discrete values. Silicone oils of viscosities $\nu = 100$, 300, 1000, and $5000\,\mathrm{cm}^2\,\mathrm{s}^{-1}$ were used, but we observed spiral patterns only for $\nu = 300\,\mathrm{cm}^2\,\mathrm{s}^{-1}$. We also used different orifice diameters ($d = 0.68$, 1.5, 1.6, and 2.5 mm). While we saw some irregular patterns for $d = 0.68\,\mathrm{mm}$ with $Q = 0.02\,\mathrm{cm}^3\,\mathrm{s}^{-1}$ and $H = 30\,\mathrm{mm}$, clear spiral patterns were observed only for $d = 1.5$ and 1.6 mm, $Q = 0.047$–$0.137\,\mathrm{cm}^3\,\mathrm{s}^{-1}$, and $H = 32$–$50\,\mathrm{mm}$.

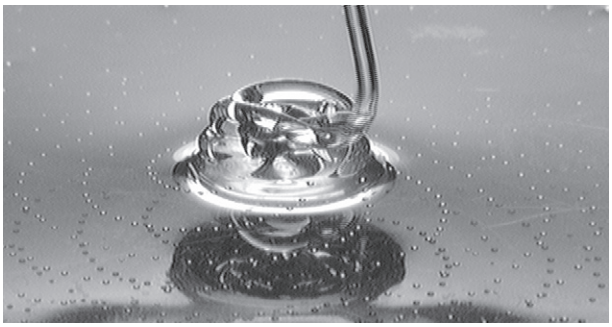

Fig. 2: Inside a quite narrow region of the control parameter space, the coiling rope traps bubbles of air which form nice spiral patterns. Notice how the subsequent coils are displaced with respect to each other. The diameter of the pile is about 1 cm.

Figure 1 shows two pictures of steady "liquid rope coiling". Depending on the fall height and the fluid viscosity, the pile of coils can have different shapes. For low fall heights and high viscosities ("viscous" regime), the pile remains intact for several coiling periods, becomes quite high, and has a shape like a corkscrew (fig. 1a). For somewhat greater heights and/or lower viscosities (called the "gravitational regime"), the pile disappears within one or two coiling periods, and remains low (fig. 1b). No bubbles are generated in either of these cases.

At still larger fall heights (called the "inertial regime"), fluid inertia becomes important. Because the coiling period is much shorter than the time required for an individual coil to coalesce completely with its predecessor, the coiling filament forms a tall liquid tube that builds up, buckles under its own weight at a critical height, and starts rebuilding again with a characteristic period [23]. In this regime we observed bubbles of two different sizes: bubbles smaller than the filament radius that form with a period comparable to that of the coiling; and larger bubbles with sizes comparable to that of the liquid tube that form during the secondary buckling. However, the patterns formed by both types of bubbles are very irregular.

Within a quite narrow portion of the gravitational coiling regime, however, encapsulated air bubbles are observed to form very regular and beautiful spiral patterns (fig. 2). The origin of this behavior is as follows. In all other coiling regimes, each newly formed coil falls exactly on top of the one laid down previously. In this small part of the gravitational regime, by contrast, the center of coiling precesses along a separate circle of its own, with a frequency much smaller ($\approx 25\%$) than that of the coiling itself. As a result, successive coils do not land exactly on top of one another; and it is at the intersections of two such coils that small air bubbles are formed and trapped

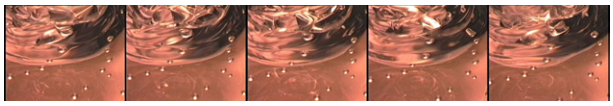

Fig. 3: The process of air trapping and bubble formation. Reflection and refraction on the curved surface of the coils makes it difficult to study the details of bubble formation, but one can still follow the dynamics as seen in this series of pictures showing one cycle of bubble formation in two branches —one just above the center of the picture, and one in the upper right corner.

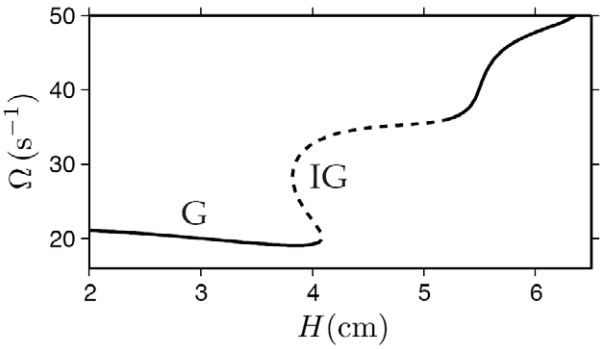

Fig. 4: Angular coiling frequency Ω *vs.* fall height H for an experiment with $\nu = 300\,\mathrm{cm^2\,s^{-1}}$, $d = 1.6\,\mathrm{mm}$, and $Q = 0.137\,\mathrm{cm^3\,s^{-1}}$, predicted numerically using the method of [20]. The symbols G and IG indicate portions of the curve corresponding to gravitational and inertio-gravitational (multivalued) coiling, respectively. The dashed portion of the curve indicates steady coiling states that are unstable to small perturbations, as determined using the method of [24]. Clear spiral patterns were observed in the height range $H = 3$–$4\,\mathrm{cm}$, before the turning point in the numerical curve that marks the onset of IG coiling [22]. The experimentally measured angular frequencies of coiling and precision were $17 \pm 1\,\mathrm{s^{-1}}$ and $4 \pm 1\,\mathrm{s^{-1}}$, respectively.

in the liquid due to its high viscosity. The spiral patterns are then generated as the bubbles are advected radially away from the pile of coils by the flow associated with the pile's gravitational collapse (fig. 3).

In our experiments, the behavior of the bubbles showed a clear progression as the fall height was increased. At relatively low heights corresponding to the lower-frequency part of the gravitational regime [20–23], the center of coiling precessed and some irregular bubbles were formed. At somewhat greater heights, the bubble pattern became more regular and some rather unclear spiral patterns were observed. At still greater heights, the patterns become clear spirals. Finally, at heights corresponding to the upper end of the gravitational regime the patterns once more became unclear and finally disappeared. The correspondence between spiral patterns and the gravitational regime is illustrated in fig. 4, which shows a numerical prediction of the steady coiling frequency *vs.* height for the parameters of one of our laboratory experiments [20]. The

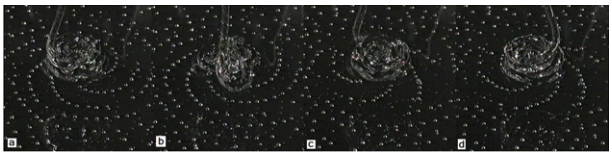

Fig. 5: Time sequence showing how a spontaneous change of coiling direction changes the sign of the curvature of the spiral pattern, for an experiment with $\nu = 300\,\mathrm{cm^2\,s^{-1}}$, $d = 1.6\,\mathrm{mm}$, $Q = 0.137\,\mathrm{cm^3\,s^{-1}}$, and $H = 4\,\mathrm{cm}$. (a) $t = 0$: coiling with spirals curving clockwise towards the center; (b) $t = 2\,\mathrm{s}$: in the middle of changing direction, with an "extra" coil outside the pile; (c) $t = 6\,\mathrm{s}$: counterclockwise coiling with a disturbed spiral pattern near the pile; (d) $t = 7\,\mathrm{s}$: completed change of direction: counterclockwise coiling and curvature of the spiral pattern.

portions of the curve corresponding to the gravitational regime and the multivalued "inertio-gravitational" regime are labelled (G) and (IG), respectively [22]. In the experiment in question, we observed clear spiral patterns in the height range $H = 3$–$4\,\mathrm{cm}$, which evidently corresponds to the gravitational regime just below the first turning point in the curve in fig. 4. This conclusion is further confirmed by our observation that the coiling frequency in the spiraling regime was nearly constant, as predicted by the numerics for $H = 3$–$4\,\mathrm{cm}$ (fig. 4). However, we emphasize that the numerical calculation leading to fig. 4 is for *steady* coiling only, without precession. The precession is due to the interaction of the free portion of the liquid rope with the pile of coils beneath it. At present this interaction is not accounted for in the boundary conditions used in the numerical calculation of the steady coiling frequency. Accordingly, fig. 4 should not be interpreted as a bifurcation diagram for (unsteady) coiling with precession. Rather, its purpose is simply to help "locate" the phenomenon of spiral waves within the now well-understood regime diagram of steady coiling.

In all cases where clear spirals are observed, the spirals have five branches, and five bubbles are generated in approximately four coiling periods. The bubble size increases with increasing flow rate and also depends on the fall height, and is larger for clear spiral patterns than for unclear ones. The curvature of the spiral branches depends on the flow rate, the fall height, and the direction of coiling. If the coiling direction is reversed after an external perturbation of the filament, the curvature of the branches changes sign (fig. 5). Changing the height leads to a change in the coiling frequency and also changes the curvature of the branches (fig. 6). While the branches are strongly curved in most of the relevant parameter region they can be nearly straight (fig. 6(c)). The curvature of the pattern also depends on the radial flow away from the pile along the surface. Thus if we modify the experiment by using a plane with boundaries at some distance from the pile, the radial flow is slower and the branches closer together.

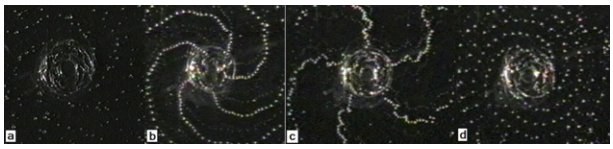

Fig. 6: Effect of fall height on the shape of the spiral branches, for an experiment with $\nu = 300\,\mathrm{cm^2\,s^{-1}}$, $d = 1.6\,\mathrm{mm}$, and $Q = 0.137\,\mathrm{cm^3\,s^{-1}}$. (a) $H = 3\,\mathrm{cm}$; (b) $H = 3.5\,\mathrm{cm}$; (c) $H = 3.7\,\mathrm{cm}$; (d) $H = 4\,\mathrm{cm}$. In all photographs, the coiling is in the same direction and the number of spiral branches is 5. Photos were taken from below; reflection of light from the glass substrate is the cause of the extra "ghost" branches.

On the basis of our experimental observations we now propose a simple model for the formation of the spirals. We have seen that the slow precession of the coiling center causes successive coils to be slightly displaced from each other, leading to the trapping of air bubbles which are subsequently transported radially with the stagnation flow. Assumptions of volume conservation and constant height of the fluid film implies that the radial position of a bubble obeys $\frac{\mathrm{d}r}{\mathrm{d}t} \sim 1/r$ or $r \sim t^{0.5}$. Since the bubble generator moves with constant angular speed, this gives $r = \pm a\theta^{0.5}$, where r is the radius, a some constant, and θ the angle. Spirals obeying this type of equation are called Fermat's spirals. To model this we assume that the coiling center moves with frequency f_p on a circle with radius r_p. If the radius and frequency of the coiling about this center are r_c and f_c, respectively, then the path laid down by the coiling filament is

$$x(t) = r_p \cos(2\pi f_p t) + r_c \cos(2\pi f_c t), \tag{1a}$$

$$y(t) = r_p \sin(2\pi f_p t) - r_c \sin(2\pi f_c t). \tag{1b}$$

We observe experimentally that the coiling and precession are always in opposite directions and since we want to keep f_c and f_p positive we include the minus sign in (1b). An example of the trajectory given by eq. (1) is shown in fig. 7.

Our experiments show that $f_c/f_p \approx r_c/r_p \approx 4$. Now if $f_c/f_p = 4$ exactly, the path defined by eq. (1) will repeat itself after one precession period and the "spirals" will be straight lines pointing outwards from the origin. If however f_c/f_p differs slightly from 4, the path will shift slightly with each precession period and a curved spiral pattern will emerge (fig. 8). As already mentioned, our numerical code does not include the interaction between the coiling rope and the pile so we do not yet understand what causes this precession. We are currently attempting to correctly include this interaction and understand how the precession frequency varies with the experimental parameters and why $f_c/f_p \approx r_c/r_p \approx 4$ for all experiments we performed. This is however far beyond the scope of the present paper. We did observe, however, that the spiral patterns change smoothly with system parameters, indicating that frequency locking does not occur. Our

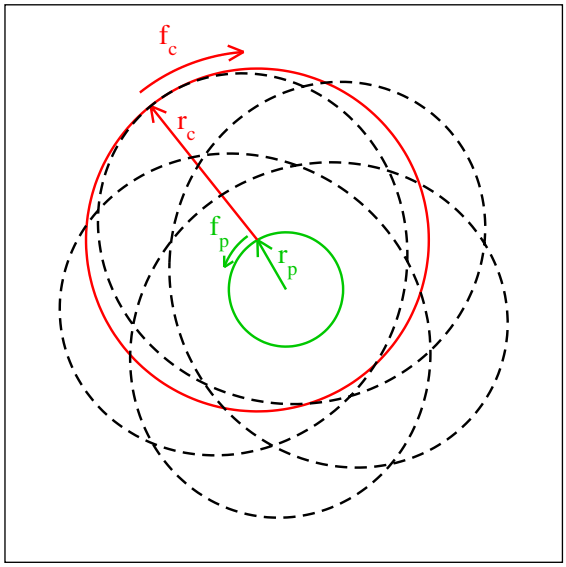

Fig. 7: Rope coiling around a center which moves on a circle of its own. r_c and f_c are the radius and frequency of coiling, while r_p and f_p are the radius and frequency of precession of the coiling center. The direction of precession is opposite to that of the coiling. A figure very similar to this one has been used to explain the meandering of spirals [5,12]. Here $r_c/r_p = 3$ and $f_c/f_p = 4$.

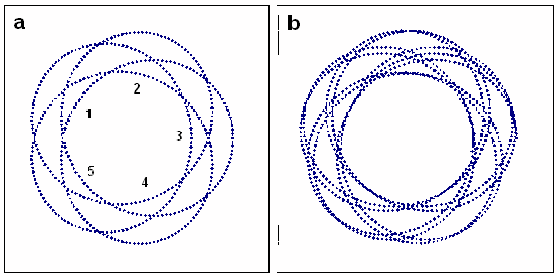

Fig. 8: A model of the path laid down by the coil for the experimentally measured values of $r_c/r_p \approx 4$ and $f_c/f_p \approx 4$. (a) When $f_c/f_p = 4$, the path exactly repeats itself, giving rise to straight radial branches (fig. 9a.) Bubbles are generated at positions 1, 2, 3, 4, and 5. (b) When $f_c/f_p = 3.9$ the path is slightly displaced after each precession period, giving rise to curved spiral branches (fig. 9b.)

experimental observations indicate that during coiling bubbles are trapped at points 1 through 5 in fig. 8, so that five bubbles will be generated for each four coils. Geometrically speaking, a bubble is formed each time the vector $\mathbf{r}_p = r_p(\hat{\boldsymbol{x}} \cos 2\pi f_p t - \hat{\boldsymbol{y}} \sin 2\pi f_p t)$ from the rotation center to the coiling center is antiparallel to the vector $\boldsymbol{r}_c = r_c(\hat{\boldsymbol{x}} \cos 2\pi f_c t + \hat{\boldsymbol{y}} \sin 2\pi f_c t)$ from the coiling center to the filament laid down (see fig. 7). The frequency of bubble formation is therefore just that of the dot product

$$\boldsymbol{r}_c \cdot \boldsymbol{r}_p = r_c r_p \cos 2\pi (f_c + f_p) t, \tag{2}$$

or $f_c + f_p$. The number of bubbles generated per coil is therefore $(f_c + f_p)/f_c$. For the measured value

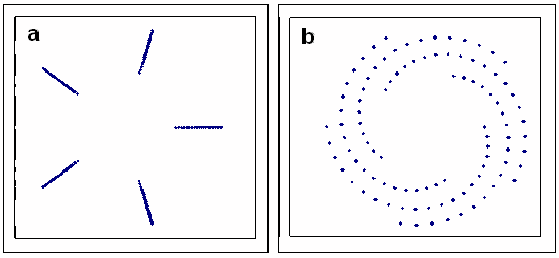

Fig. 9: Patterns of bubbles generated at positions 1, 2, 3, 4, and 5 in fig. 8. a) If $f_c/f_p = 4$ exactly the loop is closed and the bubble branches are radial. b) If f_c/f_p is only approximately 4 (here 3.9) the loop is open and the bubble branches will be curved.

$f_c/f_p \approx 4$, this gives $(f_c + f_p)/f_c \approx 5/4$, as observed in our experiments. From the frequency of bubble generation one can also predict the number of spiral branches to be $n(f_c + f_p)/f_p$, where n is the smallest natural number that makes $n(f_c + f_p)/f_p$ approximately a natural number. The factor n is present because if, *e.g.*, $f_c/f_p = 4.33$, then $(f_c + f_p)/f_p = 5.33$ and it will take three rotations of the coiling center to add a bubble to all branches and start adding to the first one again, yielding a total of 16 branches. The reason that $n(f_c + f_p)/f_p$ need not be exactly a natural number is that if it is sufficiently close, say 4.98, the bubbles will not be seen as defining 50 distinct branches but rather 5 branches that are slightly curved (see fig. 9)

To test our model against the experiments, we did a simple numerical simulation assuming that the precession frequency f_p and the coiling frequency f_c are constants and that the bubbles generated move radially with a speed $v = Q/(2\pi rh)$, where r is the radial position and h the height of the fluid film. Figure 10 shows a "fit" of this simple model to the observations for an experiment with $Q = 0.047\,\mathrm{cm^3\,s^{-1}}$, $h = 4\,\mathrm{mm}$, $f_c = 2.7\,\mathrm{Hz}$, and $f_p = 0.7\,\mathrm{Hz}$. Because h was measured less accurately than the other parameters, we adjusted its value to obtain the best fit between the experiments and the model. The excellent agreement shown in fig. 10 is obtained for $h = 3.6\,\mathrm{mm}$, very close to the measured value. We attribute the slight difference between the two values to the approximation $v = Q/(2\pi rh)$. Since the bubbles are near the top of the fluid, they will move slightly faster than the average speed assumed here. The average bubble speed assumed in the model must therefore be slightly higher than it is in reality, which requires that the assumed film thickness be slightly lower than the true value, as we found above. This simple model thus yields not only a qualitative picture, but also a quantitatively detailed understanding of the formation of the spiral bubble patterns.

In conclusion, we have shown that surprising and neatly ordered spiral bubble patterns can be formed during liquid rope coiling. In the context of liquid rope coiling, and in contrast to the general case, two frequencies are required

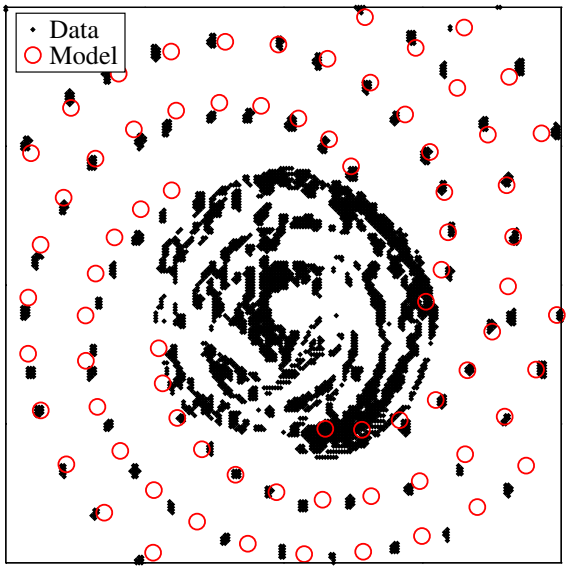

Fig. 10: A fit of the theoretical model for the bubble patterns to the observed pattern, for an experiment with $Q = 0.047\,\mathrm{cm^3\,s^{-1}}$, $h = 4\,\mathrm{mm}$, $f_c = 2.7\,\mathrm{Hz}$, and $f_p = 0.7\,\mathrm{Hz}$. The model predictions shown are those for the same values of Q, f_c and f_p but $h = 3.6\,\mathrm{mm}$.

for spiral formation, namely the frequencies of the coiling itself and that of the (retrograde) precession of the coiling center. We present a very simple model that explains how the spiral patterns are formed and why two frequencies are needed in this particular case. The specific spiral we observed is a particular type of an Archimedean spiral ($r = a\theta^{1/n}$), namely Fermat's spiral $r = a\theta^{1/2}$, which arises because the radial and angular positions of the bubbles obey $r \sim t^{1/2}$ and $\theta \sim t$.

REFERENCES

[1] Thompson D'Arcy, *On Growth and Form* (Cambridge University Press) 1917.
[2] Do Carmo M. P., *Differential Geometry of Curves and Surfaces* (Prentice-Hall) 1976.
[3] Douady S. and Couder Y., *Phys. Rev. Lett.*, **68** (1992) 2098.
[4] Douady S. and Couder Y., *J. Theor. Biol.*, **178** (1996) 255.
[5] Hakim and Karma, *Phys. Rev. E*, **60** (1999) 5073.
[6] Winfree A. T., *When Time Breaks Down* (Princeton University Press) 1987.
[7] Zykov V. S., *Modelling of Wave Processes in Excitable Media* (Manchester University Press) 1988.
[8] Jakubith S., Rotermund H. H., Engel W., von Oertzen A. and Ertl G., *Phys. Rev. Lett.*, **65** (1990) 3013.
[9] Winfree A. T., *Science*, **181** (1973) 937.
[10] Jahnke W., Skaggs W. E. and Winfree A. T., *J. Phys. Chem.*, **93** (1989) 740.
[11] Plesser T. *et al.*, *J. Phys. Chem.*, **94** (1990) 7501.

[12] Skinner G. S. and Swinney H. L., *Physica D*, **48** (1991) 1.
[13] Belmonte A., Ouyang Q. and Flesselles J. M., *J. Phys. II*, **7** (1997) 1425.
[14] Loomis W. F., *Dictyostelium Discoideum, A Developmental System* (Academic Press, New York) 1975.
[15] Siegert F. and Weijer J., *Physica D*, **49** (1991) 224.
[16] The several review articles in the focus issue of *Chaos*, **8** (1998) 1.
[17] Mahadevan L., Ryu W. S. and Samuel A. D. T., *Nature*, **392** (1998) 140.
[18] Mahadevan L., Ryu W. S. and Samuel A. D. T., *Nature*, **403** (2000) 502.
[19] Taylor G. I., *Proceedings of the 12th International, Congress of Applied Mechanics* (Springer, Berlin) 1968.
[20] Ribe N. M., *Proc. R. Soc. London, Ser. A*, **460** (2004) 3223.
[21] Maleki M., Habibi M., Golestanian R., Ribe N. M. and Bonn D., *Phys. Rev. Lett.*, **93** (2004) 214502.
[22] Ribe N. M., Huppert H. E., Hallworth M., Habibi M. and Bonn D., *J. Fluid. Mech.*, **555** (2006) 275.
[23] Habibi M., Maleki M., Golestanian R., Ribe N. and Bonn D., *Phys. Rev. E*, **74** (2006) 066306.
[24] Ribe N. M., Habibi M. and Bonn D., *Phys. Fluids*, **18** (2006) 084102.